Letter of Intent to PAC48

Measurement of the Neutral Pion Transition Form Factor and Search for the Dark-Omega Vector Boson

D. Dale[1], D. Dutta[2], L. Gan[3], A. Gasparian[4,†], I. Larin[5], N. Liyanage[6], and R. Miskimen[5]

[1] Idaho State University, Pocatello, ID 83209
[2]Mississippi State University, Mississippi State, MS 39762
3 University of North Carolina Wilmington, Wilmington, NC 28403
[4] North Carolina A&T State University, Greensboro, NC 27411
[5] University of Massachusetts, Amherst MA 01003
[6]University of Virginia, Charlottessville, VA 22904

June 22, 2020

[†] Contact person

Abstract

We propose two experiments to run concurrently using the PRad-II setup in Hall B. The first experiment is a measurement of the π^0 transition form factor (TFF) through the Primakoff reaction with virtual incident photons. The experiment has sensitivity to the TFF over a Q^2 range from .001 - 0.1 GeV^2, allowing a clean determination of the slope and curvature parameters in the TFF, and sensitivity to $\Gamma_{\pi^0\to\gamma\gamma}$, the neutral pion decay width. One of the largest uncertainties in the Standard Model prediction for the muon $g-2$ magnetic moment, hadronic light-by-light scattering, critically depends on knowledge of the pseudo-scalar meson TFFs in the low Q^2 region.

We also propose to search for a new hidden sector vector boson coupled via baryonic current (V_B or "dark omega") in the (140-620) MeV mass range. It will be produced on a Si target using high energy intense electron beams. The multi-gamma decay of this particle will be detected by a high resolution and large acceptance crystal calorimeter providing a few MeV level resolutions in $M_{\gamma\gamma\gamma}$, critically important for the signal to background separation. The motivation, feasibility studies of the setup and estimation of the realistic parameter space of the proposed experiment are discussed in this LOI.

1 Introduction

1.1 Measuring the Neutral Pion Transition Form Factor

Primakoff π^0 electroproduction can be used to measure the electromagnetic transition form factor (TFF) of the π^0 . Studies of the $\gamma^*\gamma\pi^0$ vertex, where γ^* is a virtual photon of low or moderate Q^2, enable one to study the transition regime from soft nonperturbative physics to the hard processes of perturbative QCD. The $\gamma^*\gamma\pi^0$ transition vertex has been studied theoretically from the point of view of VMD and ChPT based models, [1] [2] [3], as well as those based on treatments of the quark substructure[4] [5] [6].

The π^0 TFF is one of the measurements proposed and developed by the PrimEx collaboration for a Primakoff experimental program. This program was included in white paper documents as one of the key experiments driving the JLab 12 GeV upgrade [7, 8].

Measurements of the π^0 transition form factor at very low Q^2 (~ 0.001–$0.1 GeV^2$) can fix the slope of the transition form factor, and model independently determine the size of the neutral pion electromagnetic interaction radius. The transition is characterized by the form factor $F(-Q_1^2, -Q_2^2)$ which, if only one photon is significantly off shell with $Q^2 << m_\pi^2$, follows this parameterization,

$$F_{\gamma^*\gamma\pi^o}(-Q^2, 0) = 1 - a_\pi \frac{Q^2}{m_{\pi^0}^2} + b_\pi \Big(\frac{Q^2}{m_{\pi^0}^2}\Big)^2 \tag{1}$$

where a_π and b_π are the linear and curvature terms in the TFF, respectively.

In recent years there has been considerable interest in measurements of the pseudoscalar meson TFFs as a means to constrain hadronic corrections to the muon magnetic moment. There is currently a $3-4\sigma$ deviation between the measurement of the muons anomalous magnetic moment and the Standard Model (SM) prediction. Defining $a_\mu = (g-2)_\mu/2$ as the deviation of the magnetic moment from the value g=2 for a point-like spin-1/2 Dirac particle, the PDG experimental average and SM prediction [9] [10] for the deviation are,

$$a_\mu^{exp} = 116\ 592\ 091\ (63) \times 10^{-11} \tag{2}$$

$$a_\mu^{SM} = 116\ 591\ 820\ (36) \times 10^{-11} \tag{3}$$

New measurements in progress at FNAL (E989) and planned for J-PARC will reduce the experimental uncertainty in a_μ by a factor of four over the present value in the next few years. For this reason there has been considerable theoretical effort to reduce the error in a_μ^{SM}.

There are four classes of corrections to the SM prediction for a_μ^{SM}: (i) higher-level QED diagrams at 5-loop level, (ii) electro-weak corrections at 2-loop level, (iii) hadronic vacuum polarization (HVP) of order $O(\alpha^2)$ and $O(\alpha^3)$, and (iv) hadronic light-by-light (HLbL) corrections of order $O(\alpha^3)$. The uncertainties in the first two processes, QED and electroweak corrections, are understood to be small, $\pm 8 \times 10^{-13}$ and $\pm 1 \times 10^{-11}$, respectively, and do not limit the interpretation of the experimental results. The third class of correction, HVP, can be calculated using data driven techniques. In the data-driven approach the lowest order HVP is given by $\int K(s)R(s)/s^2\, ds$, where $\sqrt{s}$ is the C.M. energy of the e^+e^- system, K(s) is a known kinematic factor, and R(s) is given by,

$$R(s) = \frac{e^+e^- \to hadrons}{e^+e^- \to \mu^+\mu^-} \tag{4}$$

The error on HVP currently stands at $\pm 24 \times 10^{-11}$ [10]. Arguably as new measurements of $e^+e^- \to X$ improve on the determination of R, the error on HVP will decrease.

The fourth class of correction, and the one directly relevant to pseudo-scalar TFF measurements, is HLbL. The HLbL correction cannot be reduced to a data-driven form, and must be evaluated using hadronic models. The SM value for a_μ^{SM} shown in the above equation corresponds to an estimated error in a_μ^{HLbL} of $\pm 26\ \times 10^{-11}$ [10], of equal importance to the error in a_μ^{HVP} . There are two principle contributions to a_μ^{HLbL}. The first and most dominant is from the coupling of the π^0, η and η' mesons to two photons, and described by the TFFs. Data with arbitrary virtuality are needed as input to data-driven approaches and the validation of hadronic models. The next most important contribution to a_μ^{HLbL} is from double-virtual photon fusion processes $\gamma^*\gamma^* \to MM$, where $M = \pi, K, \eta$.

Vanderhaeghen and his collaborators [11] recently evaluated a_μ^{HLbL}, finding $a_\mu^{HLbL} = 87(13) \times 10^{-11}$. The individual contributions to a_μ^{HLbL} from $\gamma^*\gamma^* \to \pi^0, \eta, \eta'$ and $\gamma^*\gamma^* \to MM$, are $84(4) \times 10^{-11}$ and $-17(5) \times 10^{-11}$, respectively. Therefore, $\gamma^*\gamma^* \to \pi^0, \eta, \eta'$ largely sets the scale for a_μ^{HLbL}, while both processes make similar contributions to the total error.

1.2 A Search for the "Dark-Omega" Vector Boson

Over the last several years there has been increased theoretical and experimental activities to search for a hidden sector dark photon or A' particle in the MeV-GeV mass range, weakly coupling to the Standard Model (SM) matter through a kinetic mixing mechanism ([12] and references within). These search experiments mostly rely on an assumption that the new particle is coupling predominantly to the leptonic field. Therefore, in most of cases, they look for the production of A' in the Coulomb field of heavy nucleus and consequently decaying to leptonic pairs (e^+e^- or $\mu^+\mu^-$). On the other hand, several other additional $U(1)'$ gauge symmetries and associated vector gauge bosons were proposed soon after the electroweak $SU(2) \times U(1)_Y$ model that are one of the best motivated extensions of the SM. One successful model, a dark-sector gauge vector boson, coupling to the baryonic matter (quarks), was proposed in 1989 [13] and subsequently discussed extensively in the literature (see references in [14]). S. Tulin in his recent article ([14] by analyzing the properties of the interaction Lagrangian and requiring the low-energy symmetries of QCD, demonstrated that this new particle can be assigned the same quantum numbers as the ω meson, $J^{PC}=1^{--}$ with the leading decay channel $V_B \to \pi^0 + \gamma$ for the $M_\pi \leq M_{V_B} \leq 620$ MeV mass range. It was also suggested to search for these new particles in rare radiative decays of light neutral mesons [14, 15]. Here, we are suggesting an alternative experimental approach to search for this new particle in their direct electro-production channels in fixed-target experiments covering the same mass range.

2 Previous Measurements of the Neutral Pion TFF

We note that Danilkin et al. [11] has presented a comprehensive survey of π^0 TFF measurements across a broad range of spacelike and timelike virtualities, and we refer the reviewer to the paper for data and experimental details. Here we present just the salient measurements that are relevant to a proposed low-Q^2 spacelike measurement at JLab.

2.1 Previous Measurements in the Space-like Q^2 Region

The lowest Q^2 measurements of the π^0 TFF in the space-like region were by CELLO [16] and CLEO [17] in the Q^2 ranges 0.7-2.2 GeV^2, and 1.6-8.0 GeV^2 respectively. These measurements used the reaction $e^+e^- \to e^+e^-\pi^0$, where two photons are radiated by the colliding e^+e^- beams, one photon close to real and the second virtual, followed by $\gamma^*\gamma \to \pi^0$. Tagging either the e^+ or e^- allows for the determination of Q^2. There is also preliminary data from BESIII covering the range from 0.3 to 3.1 GeV^2 [18]. However the BESIII analysis hasn't been finalized, and efficiency corrections haven't taken radiative effects into account. Fig. 1 shows "low" Q^2 data collected to date on the spacelike π^0 TFF.

Using the technique of Padé determinates Masjuan [19] analyzed data from CELLO and CLEO, and also higher Q^2 data from Belle and BABAR. Performing a "model-independent" fit for the linear and curvature TFF parameters a_π and b_π, he obtained $a_\pi = 0.0324(12)_{stat}(19)_{sys}$ and $b_\pi = 1.06(9)_{stat}(25)_{sys} \times 10^{-3}$, an error of approximately 7%.

2.2 Previous Measurements in the Time-like Q^2 Region

The slope parameter a_π can be measured in the time-like region using the Dalitz decay $\pi^o \to e^+e^-\gamma$. The amplitude for this process is given by $F_{\gamma^*\gamma\pi^0}(q^2,0)$ with $q^2 > 0$, which in the usual linear expansion is given by,

$$F(x) = 1 + a_\pi x$$

where

$$x = \frac{m^2_{e^+e^-}}{m^2_{\pi^0}}$$

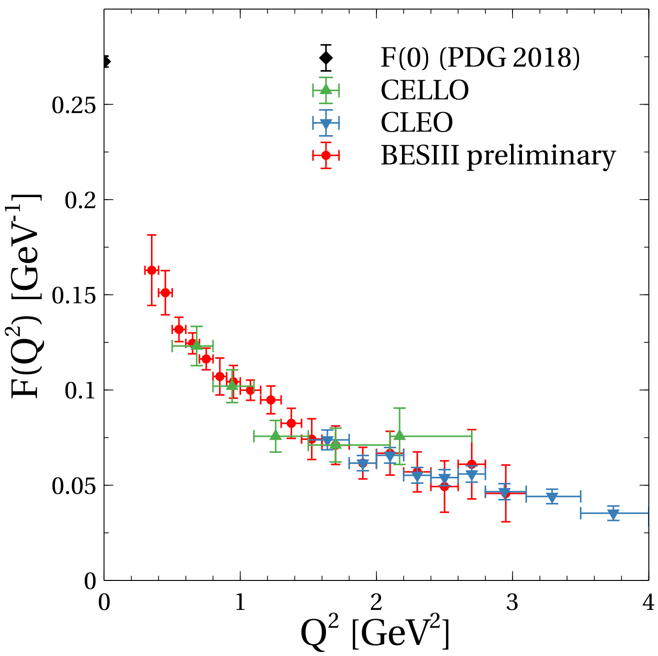

Figure 1: Momentum dependence of the spacelike π^0 TFF for $Q^2 \leq 4\ GeV^2$. Data from CELLO[16] (green triangels (up)), CLEO[17] (blue triangles (down)), and preliminary data from BESIII[18] (red circles).

The most recent measurements of a_π are from NA62 [20], based on the analysis of approximately 1.1 M $K^\pm \to \pi^0\pi^\pm$ reconstructed Dalitz decays, and from the Mainz A2 collaboration [21], based on the analysis of approximately 0.5 M $\gamma p \to \pi^0 X$ reconstructed Dalitz decays. Na62 and A2 obtained $a_\pi = .0368(51)_{stat}(25)_{sys}$, and $a_\pi = .030(10)_{total}$, respectively. The PDG has listed $a_\pi = .0335 \pm .0031$ for its average, in agreement with the analysis of Masjuan [19] A compilation of timelike slope parameter measurements is shown in Fig. 2, where $\Lambda^2 = m^2_{\pi^0}/a_\pi$.

3 Proposed Measurements

3.1 Measuring the Neutral Pion TFF

Hadjimichael and Fallieros[22] suggested that the the neutral pion form factor $|F_{\gamma^*\gamma\pi^o}(q^2_\mu)|^2$ could be accessed through the virtual Primakoff effect. The virtual Primakoff scattering

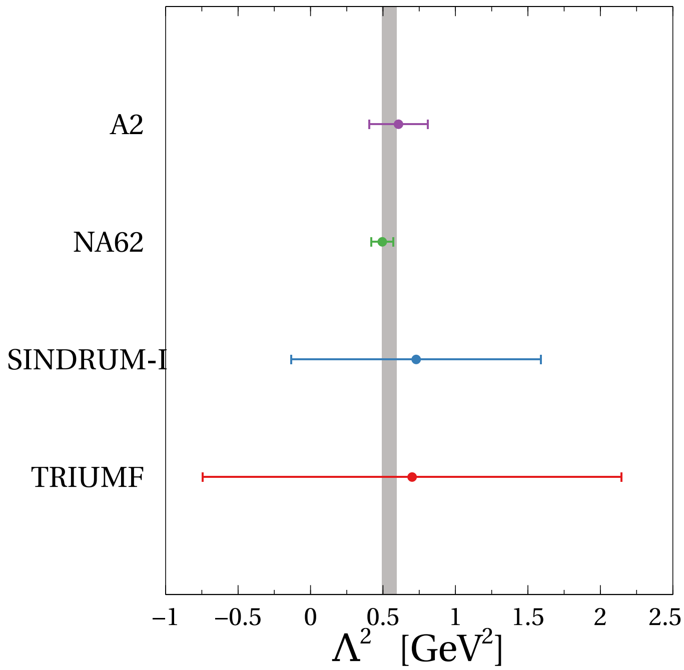

Figure 2: Slope parameter $\Lambda^2 = m^2_{\pi^0}/a_\pi$ of the timelike π^0 TFF from Dalitz decays. The gray band shows the current average value and its uncertainty listed by the PDG.

cross section is given by [22],

$$\frac{d^3\sigma_P}{d\epsilon_2 d\Omega_2 d\Omega_\pi} = \frac{Z^2\eta^2}{\pi}\sigma_M \frac{Q^4}{K^4}\frac{\beta_\pi^{-1}}{\omega_\pi}|F_N(K^2)|^2|F_{\gamma^*\gamma\pi^o}(q_\mu^2)|^2 sin^2(\frac{\theta_e}{2})sin^2(\theta_\pi)$$
$$\times[4\epsilon_1\epsilon_2 sin^2\phi_\pi + |\vec{q}|^2/cos^2(\frac{\theta_e}{2})] \quad (5)$$

where σ_M is the Mott cross section, $\eta^2 = (4/\pi m^3)/\tau$, τ is the π^o lifetime, K is the (nearly real) photon four momentum from the Coulomb field, the pion four momentum is $Q = (\vec{q}, \omega_\pi)$, $\beta_\pi = \vec{q}/\omega_\pi$, and $F_N(K^2)$ is the nuclear form factor. This expression for the cross section in similar to that for the real Primakoff effect, with the notable exception of the form factor $|F_{\gamma^*\gamma\pi^o}(q_\mu^2)|^2$ which is of interest here.

The background processes are the nuclear coherent reaction, which is coherent with the Primakoff and interferes with it, and the incoherent reaction. The nuclear coherent electro-production cross section has this structure,

$$\frac{d^3\sigma_{coherent}}{d\epsilon_2 d\Omega_2 d\Omega_\pi} \approx \eta A^2 \frac{d^3\sigma_{eN\to e'N\pi^0}}{d\epsilon_2 d\Omega_2 d\Omega_\pi} sin^2\theta_\pi |F(K^2)|^2$$

where η is the nuclear absorption factor for π^0 production, A is the atomic mass number, $d\sigma^3_{eN\to e'N\pi^0}/d\epsilon_2 d\Omega_2 d\Omega_\pi$ is the π^0 electro-production cross section on the nucleon, and $F(K^2)$ is the nuclear matter formfactor. The nuclear incoherent electro-production cross section has this structure,

$$\frac{d^3\sigma_{incoherent}}{d\epsilon_2 d\Omega_2 d\Omega_\pi} \approx \eta A\Big(1 - G(K)\Big)\frac{d^3\sigma_{eN\to e'N\pi^0}}{d\epsilon_2 d\Omega_2 d\Omega_\pi}$$

where $G(K)$ is a Pauli suppression factor, with G(0)=1 and $G(K) \to 0$ for $K > k_F$, where k_F is the nuclear Fermi momentum. The cross section summed over the three processes has this general form,

$$\frac{d^3\sigma}{d\epsilon_2 d\Omega_2 d\Omega_\pi} = \Big|\sqrt{\frac{d^3\sigma_P}{d\epsilon_2 d\Omega_2 d\Omega_\pi}} + e^{i\phi}\sqrt{\frac{d^3\sigma_{coherent}}{d\epsilon_2 d\Omega_2 d\Omega_\pi}}\Big|^2 + \frac{d^3\sigma_{incoherent}}{d\epsilon_2 d\Omega_2 d\Omega_\pi}$$

where ϕ is the complex phase between the Coulomb (Primakoff) and strong (coherent) amplitudes. In this LOI we do not present calculations for the coherent and incoherent reactions. They are similar to what has already been calculated for the PrimEx-II analysis, and will be presented in an eventual proposal. However, we note that at low Q^2 the Primakoff, coherent, and incoherent will be similar in shape and relative strength to what was seen in the PrimEx-II data. Fig. 3 shows PrimEx-II data on Si and the fit for each of these terms. It can be seen that clean separation of these processes is possible.

3.2 Search for the Dark Omega

We propose searching for V_B in direct electroproduction channels $e + A \to e' + V_B + (X) \to e' + \pi^0\gamma + (X) \to e' + \gamma + \gamma + \gamma + (X)$. These particles will be produced on a silicon target in the forward direction by a 10.5 GeV electron beam and will be identified as a "*bump*″ on the continuous experimental background of the $M_{\gamma\gamma\gamma}$ distribution. Four electromagnetic particles, e' and three decay photons will be detected in a crystal calorimeter. One of the major advantages of this experiment is that there will be a high vacuum between the solid production target and the detection system. This will allow a significant minimization of the direct (by the beam) or secondary production of known particles between the target and the detectors, which is the main source of so called "kinematical reflections", a typical problem for many search experiments. The scattered electrons, e' will be detected in forward direction ($\sim 0.5^\circ - 5^\circ$) and within an energy range of (0.5-2.5) GeV to select forward and high energy virtual photons in the reaction. That, in turn, will enhance the production of forwardly directed energetic V_B particles to boost the three decay photons to the forward calorimeter acceptance (see Sec. 6.1). We propose to run this experiment in parallel with the neutral pion form factor $F_{\gamma^*\gamma\pi^o}$ measurement at very low Q^2. Therefore, the trigger in the experiment will be formed on two levels: first level, $E_{calor} \geq 7GeV$, and second level, $N_{claster} \geq 3$.

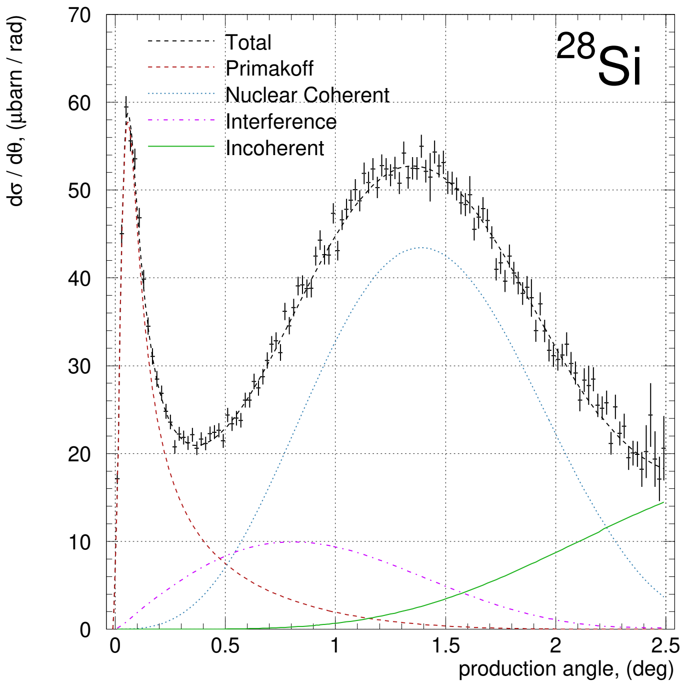

Figure 3: Si data from the PrimEx-II analysis. The curves show the Primakoff (brown), coherent (blue), interference (magenta) and incoherent (green).

4 Experimental Setup

The proposed TFF measurement and Dark Omega Search plan to use the PRad setup shown in Fig. 4, but with several critical improvements that include (i) an improved high efficiency $PbWO_4$ crystal electromagnetic calorimeter, (ii) a fADC based readout system for the calorimeter, and (iii) an additional GEM detector plane. The scattered electrons and π^0 decay photons will be detected simultaneously with high precision.

Just as in the PRad experiment the scattered electrons will travel through the 5 m long vacuum chamber with a thin windows to minimize multiple scattering and backgrounds. The vacuum chamber matches the geometrical acceptance of the calorimeter. The new GEM detectors will be placed about 40 cm upstream of the GEM detectors used in PRad, as shown in Fig. 5. The pair of GEM detector planes will ensure a high precision measurement of the GEM detector efficiency, and add a modest tracking capability to further reduce the beam-line background.

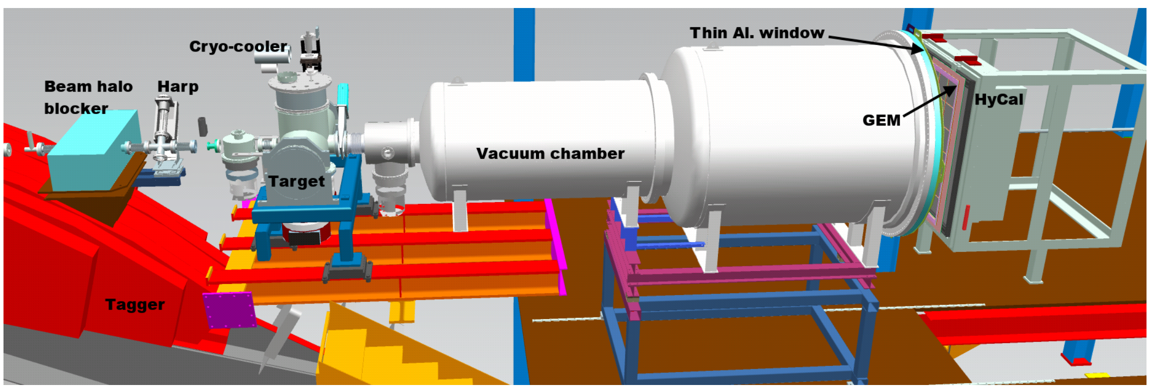

Figure 4: A schematic layout of the PRad experimental setup in Hall B at Jefferson Lab, with the electron beam incident from the left. The key beam line elements are shown along with the two-segment vacuum chamber, and the GEM and HYCAL detector systems.

The principle elements of the experimental apparatus along the beamline are as follows:

- Two stage, large area vacuum chamber with a single thin Al. window at the calorimeter end
- A pair of GEM detector planes, separated by about 40 cm for coordinate measurement as well as tracking.
- high resolution $PbWO_4$ crystal calorimeter (the Pb-glass part of the HyCal will be replaced with $PbWO_4$ crystals) with fADC based readout.

PRad-II will use an upgraded HyCal calorimeter which will be an all $PbWO_4$ Calorimeter rather than the Hybrid version used in PrimEx and PRad. The lead-glass modules of

HyCal will be replaced with new $PbWO_4$ crystals. This will significantly improve the uniformity of the electron detection over the entire experimental acceptance. Moreover, the readout electronics will be converted from a FASTBUS based system used during PrimEx and PRad to an all flash-ADC based system, which is expected to provide a seven fold improvement in the DAQ speed. A faster DAQ will allow us to collect an order of magnitude more statistics within a reasonable about of running time.

We note that the precision of the GEM detector efficiency contributed significantly to the systematic uncertainty of the PRad experiment. A high precision measurement of the GEM detector efficiency can be achieved by adding a second GEM detector plane. In this case, each GEM plane can be calibrated with respect to the other GEM plane instead of relying on the HyCal, minimizing the influence of the HyCal position resolution. It will also help reduce various backgrounds in the determination of the GEM efficiency, such as cosmic backgrounds and the high-energy photon background. In addition, the tracking capability afforded by the pair of separated GEM planes will allow measurements of the interaction $z-$vertex. This can be used to eliminate various beam-line backgrounds, such as those generated from the upstream beam halo blocker. The uncertainty due to the subtraction of the beamline background, at forward angles, is one of the dominant uncertainties of PRad. Therefore, the addition of the second GEM detector plane will reduce the systematic uncertainty contributed by two dominant sources of uncertainties.

The tracking capabilities of PRad-II will be enhanced significantly compared to PRad with the addition of a second GEM layer, 40 cm upstream of the GEM layer located next to HyCal. The new tracking layer will be built by the UVa group and the outer dimensions and readout parameters of this layer will be similar to the original PRad GEM layer; with an active area of 123 cm $\times$ 110 cm composed of two side by side detectors, each with an active area of 123 cm $\times$ 55 cm, arranged so that there is a narrow overlap area in the middle. One major improvement is that the new tracking layer will be based on the novel μRWELL technology. The biggest advantage of using this new technology for PRAd-II second tracking layer is that it would allow each detector module to be built without a spacer grid. The presence of the spacer grid in the original GEM detector caused narrow regions of lower efficiency along the spacers. While these efficiencies were measured relative to HyCal and corrected in data analysis, they contributed to the systematic uncertainty of PRad. Having spacer-less detectors as the new tracking plane will eliminate the regions of low efficiency in this new detector. Furthermore, having this spacer-less layer would allow for highly accurate determination of efficiency profile of the original GEM layer.

Important upgrades are also planned for the Hall-B beamline. The window on the Hall-B tagger is being replaced with an aluminum windows which is expected to result in a significant improvement in the beamline vacuum, particularly upstream of the target. This will help reduce one of the key sources of background observed during the PRad experiment. Further, a new beam halo blocker will be placed upstream of the Hall-B tagger magnet. This will further reduce the beam-line background critical for access to the lowest angular range and hence the lowest Q^2 range in the experiment.

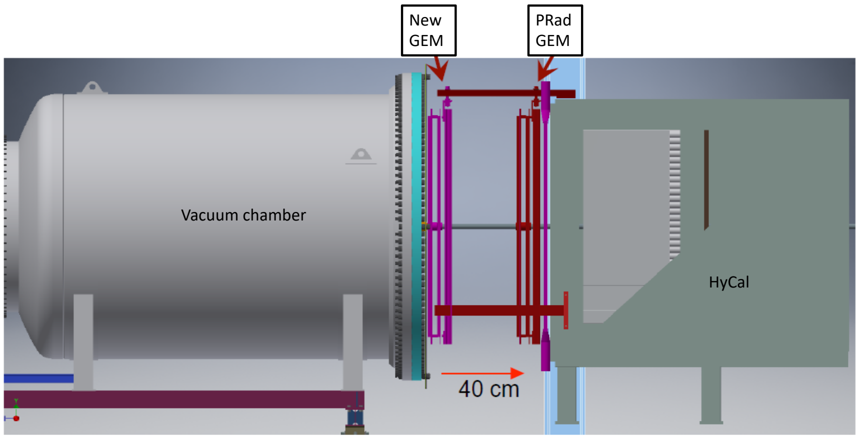

Figure 5: The placement of the new GEM chamber in the proposed experimental setup for PRad-II.

5 Expected results and uncertainties for the neutral pion TFF measurements

5.1 Event trigger

The DAQ trigger in this proposed experiment will be organized from the HyCal calorimeter requiring that at least three clusters with an energy of each greater or equal to 0.5 GeV. This type of trigger will be able to effectively select the expected three electromagnetic particles in the final stage of the reaction (the scattered electron and two decay photons from the forward produced neutral pion). The only real contamination will be from the time-accidental events from either eA-scattering and/or ee-Moller productions, both of which are high cross section processes. However, the very good timing resolution of HyCal equipped with new FADC electronics (2 ns) will make this background not essential in the DAQ trigger.

5.2 Acceptances, Resolutions, and Cross Sections

Geometric acceptances as a function of Mandelstam t are shown in Figs. 6 and 7. The plots show that the acceptance is very significant, 30% or higher, for t as low as 10^{-3} GeV^2. The acceptance as a function of Q^2 is shown in Fig. 8. Good acceptance, 50%, can be achieved for Q^2 as low as 10^{-3} GeV^2.

The π^0 invariant mass resolution, $\approx$ 2 MeV, is shown in Fig. 9. The relative Q^2 resolution, $\approx 3\%$, is shown in Fig. 10. The relative t resolution, shown in Fig. 11, sharply increases with decreasing t when reconstruction is performed purely with the calorimeter.

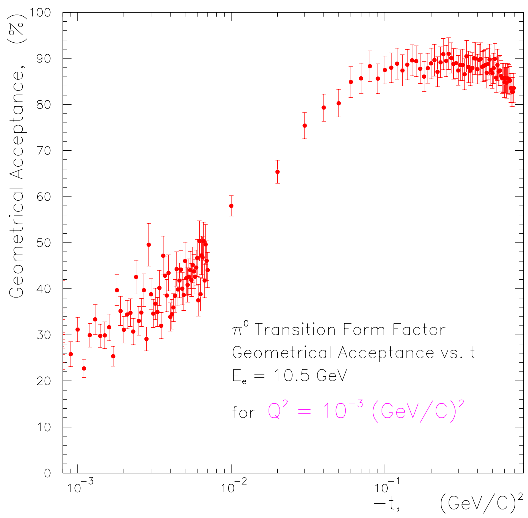

Figure 6: Geometric acceptance versus Mandelstam t for $E_0 = 10.5$ GeV and $Q^2 = 10^{-3} GeV^2/c^2$

However, when kinematic constraints are applied, the resolution is of order 10% over the range .001 - .01 GeV^2. Fig. 12 shows that the resolution in θ_π, the angle between $\vec{q}$ and $\vec{k}_\pi$, is 0.02°.

Figures 13, 14, and 15 show Primakoff cross sections as a function of the angle θ_π between $\vec{q}$ and $\vec{k}_\pi$, where $\vec{q}$ and $\vec{k}_\pi$ are the virtual photon and π^0 3-momenta, respectively. As Q^2 decreases, the Primakoff peak moves to smaller angles, which improves the separation of the Primakoff and nuclear coherent peaks. With an angular resolution in θ_π of $\sigma = 0.02°$ there will be some resolution broadening of the Primakoff peaks, particularly at low Q^2.

We conclude that the proposed experiment entirely complements the BESIII and CELLO measurements in covering the low Q^2 region with good acceptance and resolution.

6 Expected results and uncertainties for the Dark Omega search

In order to investigate the detection efficiency (including the geometrical acceptances), uncertainties in measured quantities and expected results, a full Monte Carlo (MC) simulation code based on GEANT3.21 package has been developed. This program takes into account the realistic geometry of the setup, including all resolutions of the detectors. It generates events based on estimated cross sections which are then traced through the target and detection system. The MC generated events are then analyzed to reconstruct the

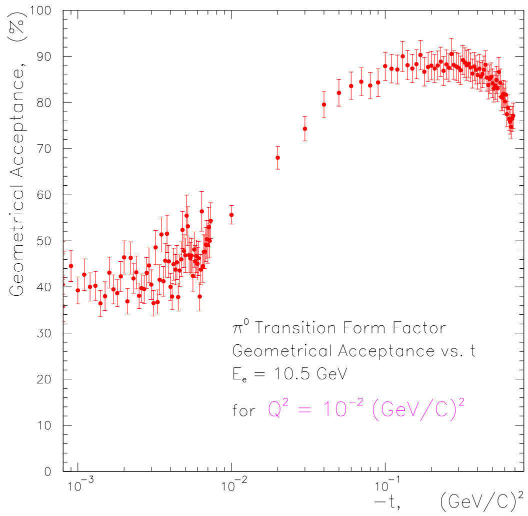

Figure 7: Geometric acceptance versus Mandelstam t for $E_0 = 10.5$ GeV and $Q^2 = 10^{-2} GeV^2/c^2$

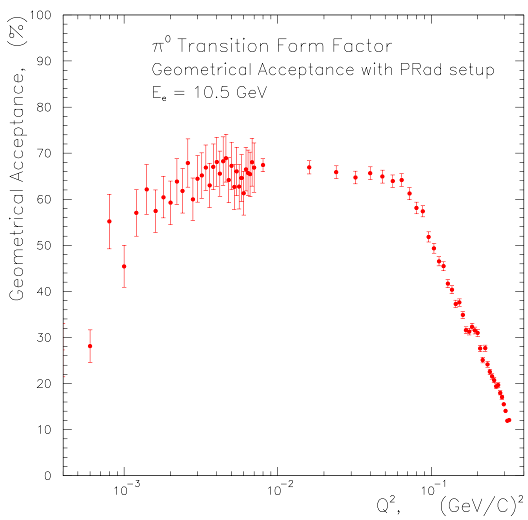

Figure 8: Geometric acceptance for PRad setup at $E_0 = 10.5$ GeV.

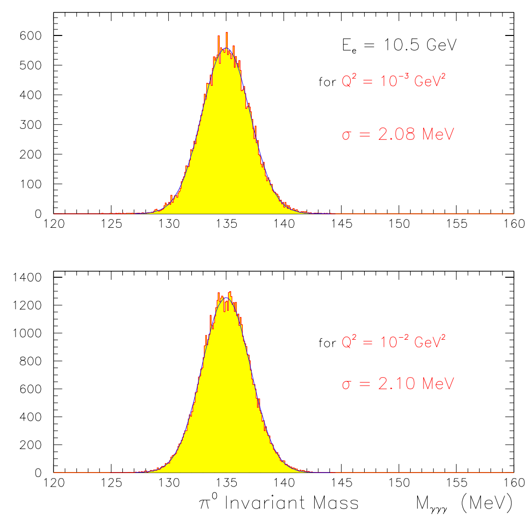

Figure 9: Invariant mass resolution at $Q^2 = 10^{-3}$ and 10^{-2} GeV$^2/c^2$

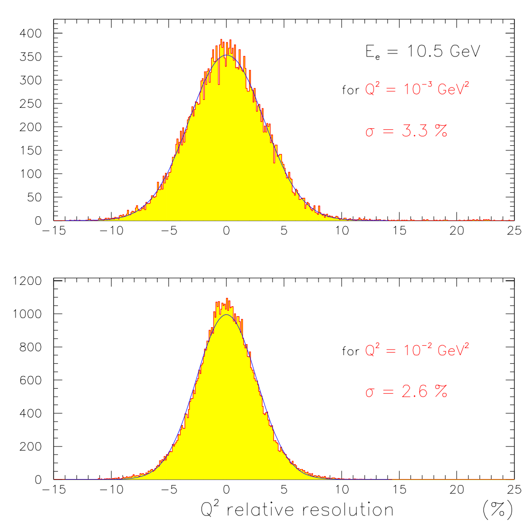

Figure 10: Relative Q^2 resolution at $Q^2 = 10^{-3}$ and 10^{-2} GeV$^2/c^2$, $E_0 = 10.5$ GeV.

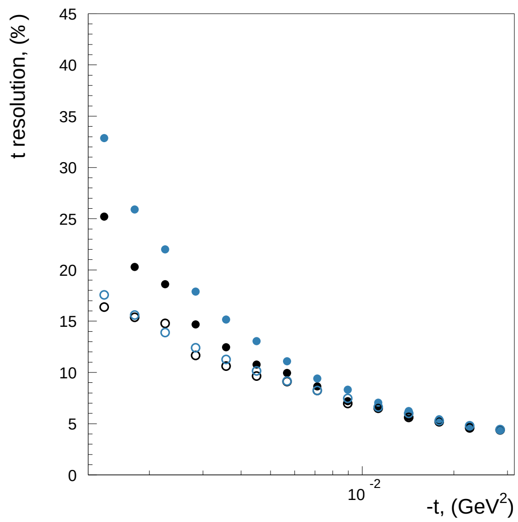

Figure 11: Relative t resolution as a function of t at $E_0 = 10.5$ GeV. The black(blue) points are at $Q^2 = .001(.01)$ GeV^2, and the filled(empty) points use reconstruction from the calorimeter(kinematic constraints).

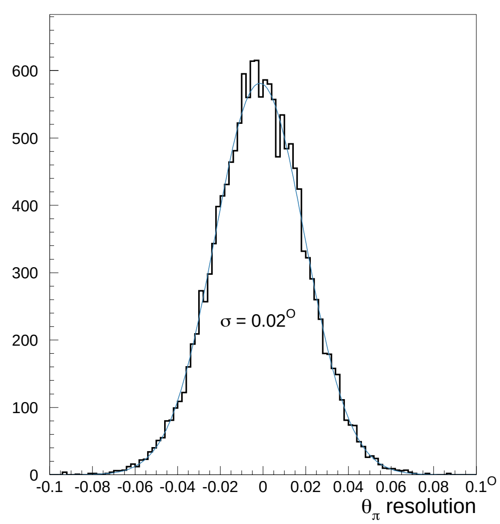

Figure 12: The resolution in θ_π $E_0 = 10.5$ GeV.

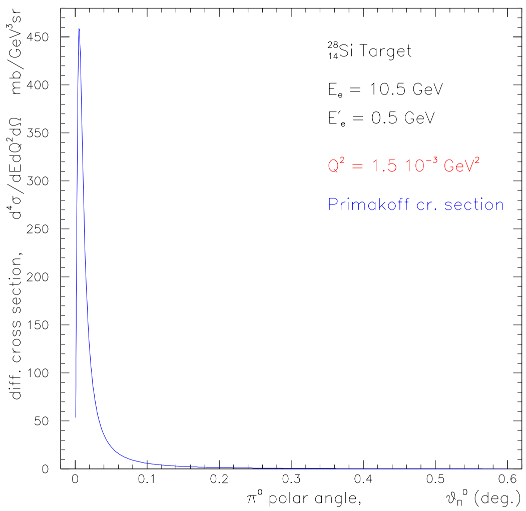

Figure 13: Primakoff differential cross section at 1.5×10^{-3} GeV^2.

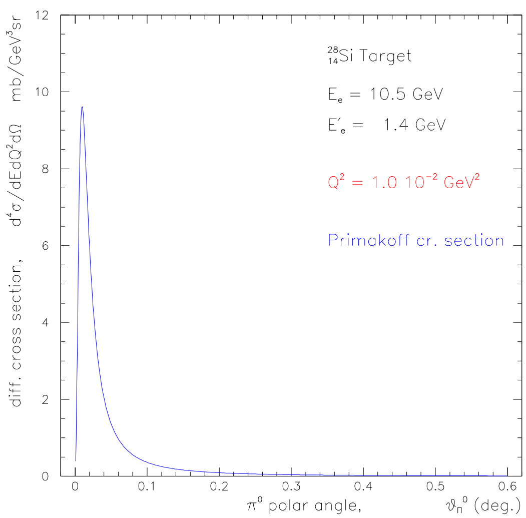

Figure 14: Primakoff differential cross section at 1.0×10^{-1} GeV^2.

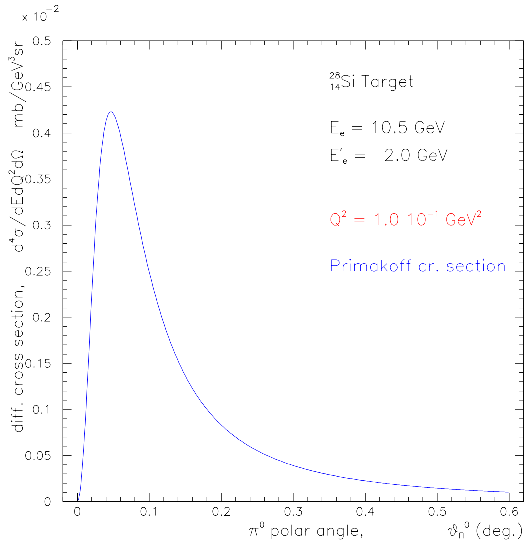

Figure 15: Primakoff differential cross section at 1.0×10^{-1} GeV^2.

"measured" experimental quantities.

6.1 Detection efficiency

Four final state particles will be detected in this experiment: the forward scattered electrons and three decay photons from V_B. The scattered electrons within the (0.5-2.5) GeV energy range will be detected in order to select energetic and forwardly directed V_B particles to maximize the detection efficiency in the experiment. A side view of a typical dark omega event is shown in Fig. 16. The simulated detection efficiency *vs.* target to calorimeter distance are shown in Fig. 17, Left. As it is seen from these simulations, the currently existing Z=5 m distance for the PRad setup, is also well optimized for this proposed experiment, with relatively large (30-60)% detection acceptances for the (140-620) MeV mass range.

6.2 Invariant mass resolution

For the fixed target to calorimeter distance (Z=5m) the HyCal position and energy resolutions are defining the $M_{\gamma\gamma\gamma}$ invariant mass resolutions. The inner $PbWO_4$ crystal part of the HyCal calorimeter has excellent energy and position resolutions: $\sigma_E/E = 2.6\%/\sqrt{E}$ and $\sigma_{x,y} = 2.5$ mm$/\sqrt{E}$ greatly improving the $M_{\gamma\gamma\gamma}$ resolution. The outer Pb-glass part of HyCal has a factor of 2 less resolution in both energy and position reconstructions. The distribution of simulated invariant masses are shown in Fig. 17, Right, for three typical

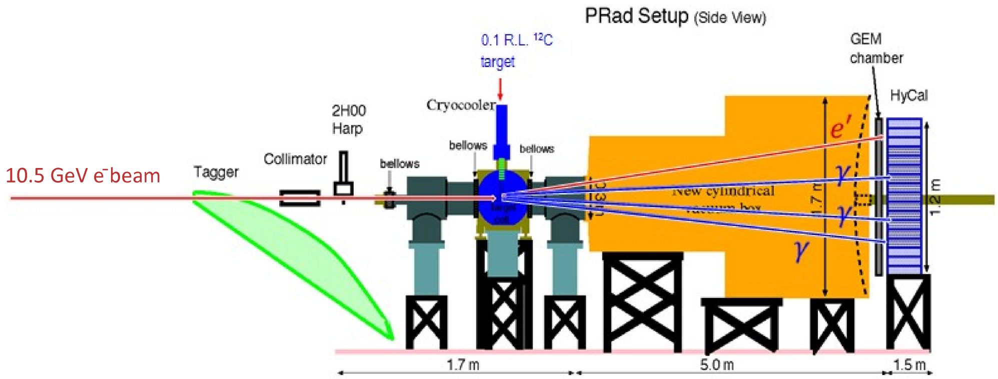

Figure 16: Side view of the proposed experimental setup, and a typical dark omega event.

values of M_{V_B}. The proposed experiment will provide an MeV-level resolutions in reconstructed M_{V_B}, which is critically important for the signal-to-background separation (see Sec. 6.5).

6.3 Displaced vertex resolution

Solid thin-targets offer an additional selection mechanism in search experiments. That requires reconstruction of the decay vertex on event-by-event bases. This usually done by additional set of tracking detectors, in cases when the decay particles are charged [12]. In the proposed experiment the decay particles are three photons, however, there is an interesting way to determine the $V_B \to \pi^0\gamma$ decay vertex by using the $\pi^0 \to \gamma\gamma$ channel, assuming that the M_{π^0} is known. An example of the simulated vertex distribution is shown in Fig. 18, Left for M_{V_B}=400 MeV particles produced in forward direction. Though, our resolutions on this particular selection criterion (cm-level) are not as good as in the case of the charged-particle tracking [12], it can still be used very effectively in search experiments testing different ranges of coupling constants and mass (see Fig. 19).

6.4 Experimental backgrounds

The detection system in this experiment will be able to separate photons from the electromagnetic charge particles in the final states (using GEM and HyCal). Therefore, only events with three energetic photons ($E_\gamma > 0.5 GeV$) in final state will be considered as a background process *vs.* signal events. The potential sources of the background events are: (a) accidental coincidences of events with multi-photon bremsstrahlung processes (beam background); (b) production of particles decaying into three or more energetic photons (physics background). At this stage we have identified and simulated two major physics processes contributing to the physics background: forward electro-production of $2\pi^0$ mesons

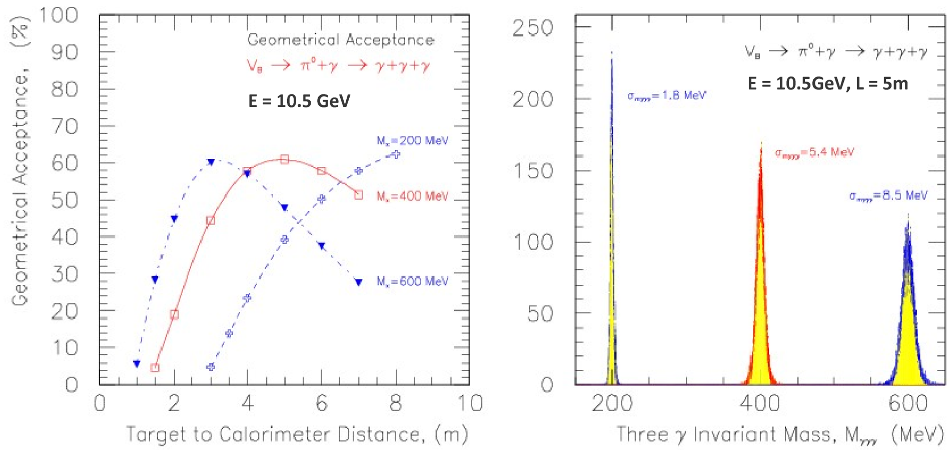

Figure 17: Left: Detection efficiency *vs.* Z for three typical M_{V_B} masses. Right: Distribution of reconstructed invariant mass for three M_{V_B}: 200 MeV, 400 MeV and 600 MeV.

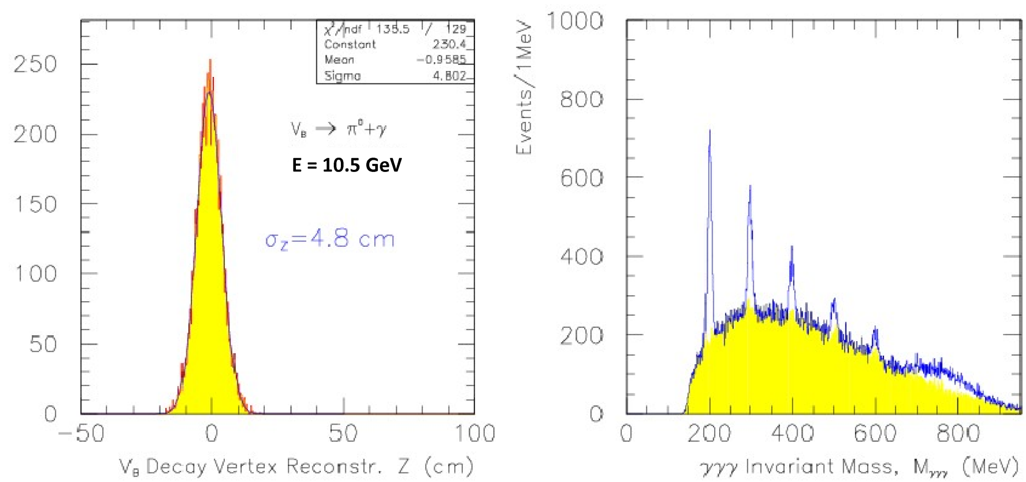

Figure 18: Left: Distribution of reconstructed vertex position. Right: Distribution of total physics background *vs.* $M_{\gamma\gamma\gamma}$. The $2\pi^0$ production process is the dominant background for this experiment (the yellow shaded area), the $\rho \to \pi^0\gamma$ background is the small bump at (650-850) MeV range. The five narrow distributions are the signal events simulated for M_{V_B}= 200, 300, 400, 500 and 600 MeV.

from the target and second, forward production of ρ mesons with their consequent decay into $\pi^0\gamma$. In both cases the π^0's decay into 2γ. The results of MC simulations for two physics background processes are shown in Fig. 18, Right, for 10 days of beam time (with E_e=10.5 GeV, $I_e = 0.1\mu$A, and 0.1% R.L. ^{12}C target). The beam background was also simulated, it has a typical exponential drop *vs.* $M_{\gamma\gamma\gamma}$ with an order of magnitude smaller than the physics backgrounds (not shown in Fig. 18).

6.5 Sensitivity of the proposed experiment

For the simulation of signal events the V_B production cross sections are required. Currently, theoretical activities are in progress to estimate these cross sections based on realistic models [23]. At this stage, based on general physics considerations, we assumed that these cross sections can be estimated by [24]: $\sigma(\gamma+P \to V_B+X) \sim (\alpha_{em}/\pi)(\alpha_B/\alpha_{em})(M_\omega/M_B)^2\sigma(\gamma+P \to hadrons)$. Then, if we take for $\sigma(\gamma + P \to hadrons) \sim 1\mu$b, we obtain $\sigma(\gamma +^{12} C \to V_B + X) \sim 1$ pb for V_B coupling constant $\alpha_B = 10^{-8}$ and mass M_B=200 MeV. The corresponding experimental yields simulated for 10 days of beam time (E_e=10.5 GeV, $I_e = 0.1\mu$A, 0.1% R.L. ^{12}C target) are shown in Fig. 18, Right for five different masses of V_B boson. These yields are shown on the top of estimated backgrounds simulated under the same conditions. The sensitivity of this experiment to search for V_B bosons on 5σ level is plotted in Fig. 19 (short-dash red line). This proposed experiment, as it can be seen from the plot, has a good potential to improve the exclusion limits on the coupling constant, α_B for about one order of magnitude *vs.* other experiments/projects (other exclusion limits in Fig. 19 are discussed in [14]).

7 Data Rates

7.1 Neutral Pion TFF

We expect the limitation on the experimental luminosity, atoms/cm$^2\times$ I$_e$, will be fixed by the ability of the PbWO4 crystal detectors to count individual signals without a significant "pile-up" effect (0.1 MHz), especially those crystals closest to the beam line. The MC simulations shown in Fig. (singles rate vs. target thickness and beam intensity) indicate that the safest combination for the proposed experiment will be to run with a 25 μm (0.025 % r.l.) Si target and 100 nA electron beam current.

To estimate the integral event rate for the Primakoff events we ran MC simulations with the following fixed parameters and intervals:

- Target: 25 μm silicon
- Beam energy: E$_e$ = 10.5 GeV
- Beam current: 100 nA

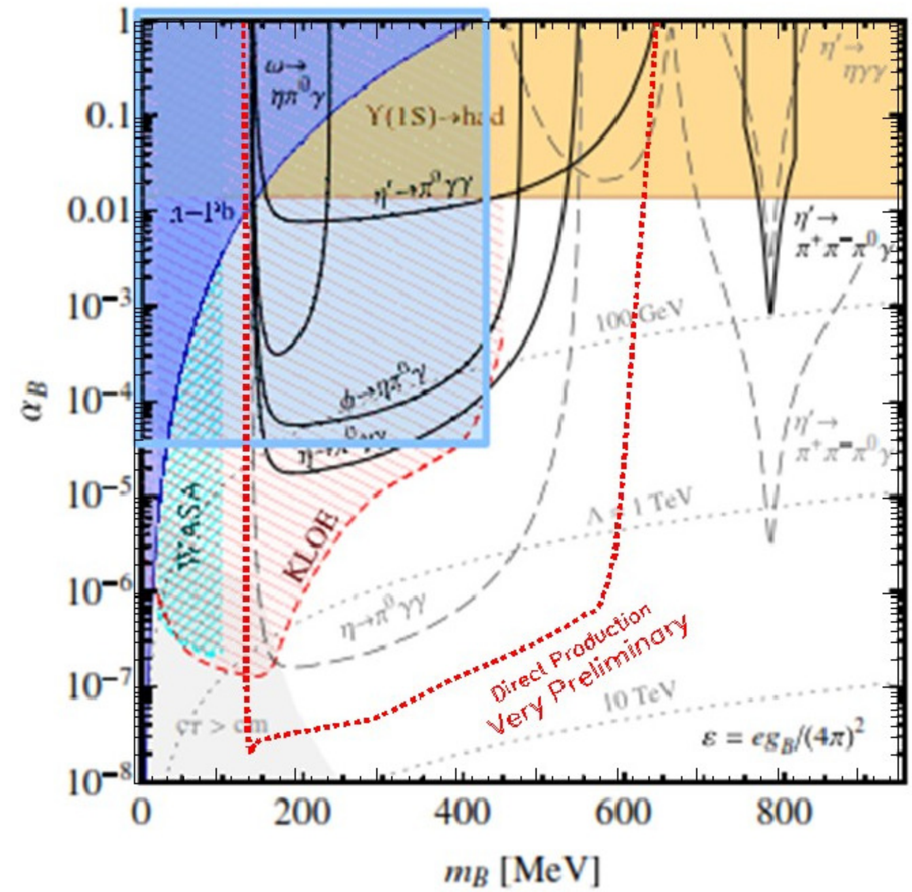

Figure 19: Current exclusion regions on V_B boson coupling *vs.* mass. The sensitivity region of the proposed experiment is shown with short-dash red line. For discussion of other exclusion limits see [14]).

- Energy range of the scattered electrons: 0.5 to 2.5 GeV
- Full range of expected Q^2 range: 10^{-3} to 0.1 GeV^2

The total integrated Primakoff cross section was estimated to be $\Delta\sigma = 1.810^{-4}$ μb. With these numbers, and an average geometrical acceptance of 50 % the event rate in the proposed experiment is:

$N_{rate} = N_e \times N_{Si} \times \Delta\sigma \times \epsilon_{geom}$

$\approx 6.25 \times 10^{11} e/s \times 1.25 \times 10^{20} atoms/cm^2 \times 1.8 \times 10^{-4} \times 10^{-30} cm^2 \times 0.5$

$\approx 865\ event/day$

$\approx 26,000\ event/30\ days$

Therefore, for an estimated 30 days of beam time we will be able to accumulate a total of approximately 26,000 useful events for the entire Q^2 range from 10^{-3} to 0.1 GeV^2.

7.2 Search for Dark Omega

Event rate estimation for the Dark-Omega seach.

- Target (same as for the TFF experiment): $25\mu m$ Si, $N_{Si} = 1.25 \times 10^{20} atoms/cm^2$
- Beam intensity (the same as for the TFF): 100 nA, $I_e = 6.25 \times 10^{11} e/s$
- Geometrical acceptance: $\epsilon \approx 50\%$
- Total integrated cross section for Dark-Omega with mass M=300 MeV: $\Delta\sigma = 5pb = 5 \times 10^{-36} cm^2$

Then the event rate is given by : $N_{rate} = N_{Si} \times I_e \times \Delta\sigma \times \epsilon$

$\approx 1.2510^{20} \times 6.25 \times 10^{11} \times 5 \times 10^{-36} \times 0.5$

$\approx$ 17 event/day

$\approx$ 500 events/30 days

8 Summary

We have presented two experiments that would run concurrently using the PRad-II setup in Hall B. The first experiment is a measurement of the π^0 TFF through the Primakoff reaction with virtual incident photons. Both the scattered electron and the two decay photons will be detected in HYCAL, with GEMs used for electron tracking. The proposed measurement has sensitivity to the TFF over a Q^2 range from .001 - 0.1 GeV^2, allowing a clean determination of the slope and curvature parameters in the TFF, and complementing the spacelike BESIII and CELLO measurements at $Q^2 > 0.3$ GeV^2, and Dalitz decay measurements in the timelike region. The cross sections are proportional $\Gamma_{\pi^0 \to \gamma\gamma}$, the neutral pion decay width, and we will also pursue this as an experimental goal if feasible. We note that hadronic light-by-light scattering, one of the largest uncertainties in the Standard Model prediction for muon $g-2$, critically depends on knowledge of the pseudoscalar meson TFFs in the low Q^2 region.

Concurrently with the TFF measurement we would run a new fixed-target experiment to search for hidden sector leptophobic particles, V_B in the (140-620) MeV mass range. These particles will be produced in a low-Z target by an 10.5 GeV electron beam and detected by their $V_B \to \pi^0\gamma \to \gamma\gamma\gamma$ decay channel. The forward scattered electrons ($\sim 1.$ GeV) and three decay photons will be detected by the high resolution and large acceptance HyCal calorimeter. A narrow resonance (~ 3 MeV) over the continuum experimental background will signal observation of these particles. The capability of vertex reconstruction (though with a moderate resolutions) will add a new dimension in filtering the background processes. These types of direct production experiments are fully complimentary to already suggested projects to search in rare radiative decays of light mesons [15].

References

[1] A. Bramon J. Bijnens and F. Cornet. *Phys. Rev. Lett.*, 61:1453, 1988.

[2] B. Moussallam. *Phys. Rev. D*, 51:4939, 1995.

[3] F. Cornet J. Bijnens, A. Bramon. *Z. Phys. C*, 46:599, 1990.

[4] L.G. Landsberg. *Phys. Rep.*, 128:302, 1985.

[5] P. Maris and P.C. Tandy. *Nuclear Physics A*, 663, 2000.

[6] M.R. Frank et al. *Phys. Lett. B*, 359:17, 1995.

[7] *The Science Driving the 12 GeV Upgrade of CEBAF, https://www.jlab.org/div dept/physics division/GeV/WhitePaper V11.pdf*, 2001.

[8] *Conceptual Design Report (CDR) for the Science and Experimental Equipment for the 12 GeV Upgrade of CEBAF, https://www.jlab.org/div dept/physics division/GeV/doe$_r$eview/CDRforScienceReview.pdf*, 2005.

[9] F. Jegerlehner. *Springer Tracts Modern Phys.*, 274:030001, 2017.

[10] A. Keshavarzi et al. *Phys. Rev. D*, 97:114025, 2018.

[11] I. Danilkin et al. *Prog. Part. Nucl. Phys.*, 107:20, 2019.

[12] *HPS Proposal,* $http://www.jlab.org/exp_prog/proposals/11/PR12-11-006.pdf$.

[13] A. Nelson and N. Tetradis. *Phys. Lett. B*, 221:80, 1989.

[14] S. Tulin. *Phys. Rev. D*, 89:114008, 2014.

[15] L. Gan et al. *JLab Prop. E12-14-004,* $http://www.jlab.org/exp_prog/proposals/14/PR12-14-004.pdf$.

[16] H. J. Behrend et al. (CELLO Collaboration). *Z. Phys. C*, 49:401, 1991.

[17] J. Gronberg et al.(CLEO Collaboration). *Phys. Rev. D*, 57:33, 1998.

[18] C.F. Redmer (BESIII Collaboration). *13th Conference on the Intersections of Particle and Nuclear Physics*, 2018.

[19] P. Masjuan. *Phys. Rev. D*, 86:094021, 2012.

[20] Lazzeroni et al. *Phys. Lett. B*, 768:38, 2017.

[21] P. Adlarson (A2 Collaboration). *Phys. Rev. C*, 95:035208, 2017.

[22] E. Hadjimichael and S. Fallieros. *Phys. Rev. C*, 39:1438, 1989.

[23] S. Tulin. *private communication.*

[24] M. Pospelov. *private communication.*